

Archaeometric analysis of patinas of the outdoor copper statue Sant'Oronzo (Lecce, Italy) preparatory to the restoration

*Original*

Archaeometric analysis of patinas of the outdoor copper statue Sant'Oronzo (Lecce, Italy) preparatory to the restoration / Buccolieri, G.; Castellano, A.; Serra, A.; Zavarise, G.; Palmiero, E.; Buccolieri, A.. - In: MICROCHEMICAL JOURNAL. - ISSN 0026-265X. - STAMPA. - 154:104538(2020). [[10.1016/j.microc.2019.104538](https://doi.org/10.1016/j.microc.2019.104538)]

*Availability:*

This version is available at: 11583/2787076 since: 2020-01-30T14:41:25Z

*Publisher:*

Elsevier Inc.

*Published*

DOI:[10.1016/j.microc.2019.104538](https://doi.org/10.1016/j.microc.2019.104538)

*Terms of use:*

This article is made available under terms and conditions as specified in the corresponding bibliographic description in the repository

*Publisher copyright*

(Article begins on next page)

1  
2  
3  
4  
5  
6  
7  
8  
9  
10  
11  
12  
13  
14  
15  
16  
17  
18  
19  
20  
21  
22  
23  
24  
25  
26  
27

# Archaeometric analysis of *patinas* of the outdoor copper statue *Sant'Oronzo* (Lecce, Italy) preparatory to the restoration

Giovanni Buccolieri<sup>a</sup>, Alfredo Castellano<sup>a</sup>, Antonio Serra<sup>a</sup>, Giorgio Zavarise<sup>b</sup>,  
Elisabetta Palmiero<sup>c</sup>, Alessandro Buccolieri<sup>d,\*</sup>

<sup>a</sup> Dipartimento di Matematica e Fisica, University of Salento, Lecce, Italy

<sup>b</sup> Dipartimento di Ingegneria Strutturale, Edile e Geotecnica, Politecnico di Torino, Torino, Italy

<sup>c</sup> Restauratrice dell'Azienda Colaci Emilio, Impianti e Restauri, Alessano, Lecce, Italy

<sup>d</sup> Dipartimento di Scienze e Tecnologie Biologiche e Ambientali, University of Salento, Lecce, Italy

\* Corresponding author. A. Buccolieri, Dipartimento di Scienze e Tecnologie Biologiche e Ambientali, University of Salento, Lecce, Italy. E-mail: [alessandro.buccolieri@unisalento.it](mailto:alessandro.buccolieri@unisalento.it)

## Abstract

28 The *Sant'Oronzo* statue (Lecce, Southern Italy) consists of an internal wooden structure, completely  
29 covered with copper sheets, lying on a concrete base about 1.5 meters high, which is placed on the  
30 top of a Roman column about 29 meters high. Lecce may be classified as urban site since it is mainly  
31 influenced by vehicular traffic and it is not affected by intense industrial emissions.

32  
33 In the time schedule of the restoration, first of all, non-destructive analyses were planned. In  
34 particular, a portable energy dispersive X-ray fluorescence (ED-XRF) was used in order to map the  
35 composition of the *patinas* and to evaluate their degradation. Subsequently, a micro-sampling was  
36 performed both of the statue and the column. The collected samples were analysed by using Raman  
37 spectroscopy and X-Ray Diffraction in order to evaluate chemical composition.

38  
39 This paper summarizes the archaeometric results and the diagnostic information obtained before of  
40 the restoration, which are significant for the restorers' subsequent work.

41  
42  
43  
44  
45  
46  
47 **Keyword:** outdoor statue, copper, *patina*, ED-XRF, Raman, XRD

## 1. Introduction

48  
49  
50  
51  
52  
53 The *patina* of outdoor copper manufacture has different chemical composition depending on the several  
54 parameters such as alloy composition, environmental conditions (for instance, urban, rural, marine,  
55 industrial), location of statue (in exposed areas or sheltered areas) and exposure time [1–4]. In  
56  
57  
58  
59

60 particular, in urban atmospheres, *patinas* directly exposed to rain are unstable and are leachable by  
61 rainwaters.  
62

63  
64 The *patinas* spontaneously develop over time on copper and bronze surfaces due to chemical  
65 reactions with the environment, creating corrosion compounds with various color (for example  
66 green, red, bluish, brown and black) and different composition such as copper oxide, copper sulfide,  
67 copper chloride, copper sulfate and copper carbonate [5–9]. In particular, the degradation compounds  
68 most commonly found in copper manufactures are  $\text{Cu}_2\text{O}$  (cuprite),  $\text{CuO}$  (tenorite),  $\text{Cu}_2\text{S}$  (chalcocite),  
69  $\text{CuS}$  (covellite),  $\text{CuCl}$  (nantokite),  $\text{CuCl}_2 \cdot 2\text{H}_2\text{O}$  (eriochalcite),  $\text{Cu}_2\text{Cl}(\text{OH})_3$  (atacamite),  $\text{Cu}_2\text{Cl}(\text{OH})_3$   
70 (botallackite),  $\text{Cu}_2\text{Cl}(\text{OH})_3$  (clinoatacamite),  $\text{Cu}_3\text{SO}_4(\text{OH})_4$  (antlerite),  $\text{Cu}_4\text{SO}_4(\text{OH})_6$  (brochantite),  
71  $\text{Cu}_2\text{OSO}_4$  (dolerophanite),  $\text{Cu}_4\text{SO}_4(\text{OH})_6 \cdot 2\text{H}_2\text{O}$  (langite),  $\text{Cu}_4\text{SO}_4(\text{OH}) \cdot 6\text{H}_2\text{O}$  (posnjakite),  
72  $\text{Cu}_4\text{SO}_4(\text{OH}) \cdot 2\text{H}_2\text{O}$  (wroewulfite),  $\text{Cu}_2(\text{CO}_3)(\text{OH})_2$  (malachite),  $\text{Cu}_3(\text{CO}_3)_2(\text{OH})_2$  (azurite) [10–12].  
73  
74 Jambor *et al.*, 1996 [13] reported for the first time the clinoatacamite, a new mineral polymorph of  
75  $\text{Cu}_2\text{Cl}(\text{OH})_3$ . Therefore, previous reports on paratacamite should probably be assigned to  
76 clinoatacamite instead. The polymorphs  $\text{Cu}_2\text{Cl}(\text{OH})_3$  (atacamite, paratacamite and clinoatacamite),  
77 in combination with different hydroxy sulfates and cuprite, are dominant in the black sheltered areas,  
78 while rain-washed green areas mainly consist of brochantite and cuprite [5,14,15].  
79

80  
81 The chemical composition of alloy and *patina* of copper or bronze can be determined using various  
82 analytical methods such as energy dispersive X-ray fluorescence (ED-XRF), Raman spectroscopy,  
83 scanning electron microscopy-energy dispersive X-ray (SEM-EDX), X-ray diffraction (XRD) and  
84 atomic absorption spectroscopy (AAS). Nevertheless, methodologies often favoured in the field of  
85 cultural heritage are non-destructive and portable techniques.  
86

87  
88 This work describes the experimental results of the diagnostic analysis performed on the  
89 *Sant'Oronzo* statue (Lecce, Southern Italy) before starting the restoration in June 2018.  
90

91  
92 Lecce ( $40^\circ 21' \text{ N}$ ;  $18^\circ 10' \text{ E}$ ; 30 m above sea level) has about 95 thousand inhabitants and it is about  
93 20 km away from both the Adriatic Sea and Ionian Sea. The town may be classified as urban site  
94 since it is mainly influenced by vehicular traffic [16,17]. Fig. 1 shows some photos of the statue,  
95 which highlight serious state of degradation of the copper sheet, of the Roman column and of the  
96 concrete base.  
97

## 98 99 100 101 102 103 104 105 106 107 108 **2. Materials and methods**

### 109 110 111 **2.1. Description of statue**

112  
113 The *Sant'Oronzo* statue was built in Venice in 1739 and it is 4.90 meters high. It has an internal  
114 wooden structure, completely covered with copper sheets, which were held together by copper nails.  
115

119 The thickness of copper sheets is equal to about 1 mm. The original copper nails are about 2 to 5 cm  
120 long (Fig. S1).  
121  
122

123 The statue is placed in *Sant'Oronzo* square, in the center of Lecce (Southern Italy), on a recent  
124 concrete base (2.65 m × 2.65 m) about 1.5 meters high, which is positioned on a Roman column  
125 about 29 meters high. The bottom of the statue is covered with a sheet of lead, which sit on the  
126 concrete base.  
127  
128

129 The last restoration was performed in years 1982 to 1987. In the last restoration, several copper rivets  
130 (with a steel nail, see Fig. S2) have been added to keep together the copper foils (Fig. S3).  
131 Unfortunately, the use of these rivets induced galvanic corrosion phenomena, which are visible to the  
132 naked eye. In fact, a close visual examination of statue allows to highlight two principal typologies  
133 of *patinas*: light green *patina* (in areas exposed to leaching) and dark *patina* (in areas not exposed to  
134 leaching), in addition to the numerous red drips, in correspondence of the rivets. Moreover, the  
135 column shows both green and dark dripping on concrete basement and on Roman capital.  
136  
137  
138  
139

140 On January 30, 2019 the statue was removed and transferred for restoration to *Palazzo Carafa*, the  
141 municipal building of Lecce, nearby the original site. Fig. S4 shows a picture of the statue in the  
142 room where it will be restored.  
143  
144  
145

## 146 147 **2.2. Methods**

### 148 149 **2.2.1 ED-XRF**

150 EDXRF portable equipment, which was assembled in our laboratory, is composed by an X-ray tube  
151 (MOXTEK Inc., USA) with palladium anode air-cooled and by a detector Si-PIN (Amptek Inc.,  
152 USA). The detector has a resolution of energy of about 180 eV at 5.9 keV. The output of the X-ray  
153 tube is collimated and the analyzed area has a diameter of about 3 mm [18,19]. For each measuring  
154 point, three EDXRF spectra were acquired, with acquisition time of 60 seconds and with a tube  
155 voltage of 6 kV at 40 μA and of 20 kV at 3 μA.  
156  
157  
158  
159

160 Five standard samples, with known chemical compositions, were used to calibrate the apparatus and  
161 to obtain reliable experimental data. For standards preparation, copper (II) sulphate pentahydrate  
162 ( $\text{CuSO}_4 \cdot 5\text{H}_2\text{O}$ ), copper (II) chloride dihydrate ( $\text{CuCl}_2 \cdot 2\text{H}_2\text{O}$ ), copper (I) oxide ( $\text{Cu}_2\text{O}$ ), copper (II)  
163 sulfide ( $\text{CuS}$ ) and iron powder have been used. All chemical compounds were purchased from  
164 Sigma-Aldrich® with analytical grade.  
165  
166  
167  
168

169 Each standard was prepared by mixing the compounds in different weight percentages. The use of  
170 different compounds with the same elements, but in different oxidation state, is irrelevant from the  
171 point of view of the XRF analysis, but has allowed to obtain the calibration samples at different  
172  
173  
174  
175  
176  
177

178 concentrations. In particular, the chemicals compounds have been weighted by using an analytical  
179 balance KERN model ABT 100-5M, subsequently mixed and homogenized in an agate mortar for  
180 ten minutes and finally compressed at 200 bar for ten minutes. The homogeneity of elements in the  
181 standard meets the requirements for the EDXRF quantitative analysis. Moreover, the samples  
182 analysed are supposed to “*infinite thickness*” and therefore the quantitative results are expressed in  
183 terms of weight percentage (% wt).  
184

185 Copper, sulphur, chlorine and iron were determined, for each measurement point, in order to  
186 individuate the chemical composition of the *patinas*. The description of each measurement point is  
187 summarized in [Table 1](#). The values of detection limit, all reported in wt %, for copper, sulphur,  
188 chlorine and iron are equal to 1.0, 0.5, 0.5 and 0.5 respectively. The software Microcal Origin  
189 Professional® has been used to elaborate the experimental data obtained [20].  
190

### 191 **2.2.2 Raman spectroscopy**

192 Raman analysis was performed on seven samples to identify *patina* composition. [Fig. 1](#) shows the  
193 sampling point of each sample whose characteristics are described in [Table 2](#). The samples were  
194 pounded to a fine powder in an agate mortar, homogenized and subsequently analyzed. Raman  
195 analyses were achieved by using a spectrometer Renishaw model Invia (spectral resolution:  $0.5\text{ cm}^{-1}$ ;  
196 spectral range:  $100 - 3700\text{ cm}^{-1}$ ) with an argon-ion laser ( $\lambda = 514.5\text{ nm}$ ) and a LEICA  
197 metallographic microscope. The laser beam was focused on the sample with 15 mW of excitation  
198 power. The spectra were acquired for 20 accumulations by 100 s and repeated on five different  
199 points. Then an average of Raman spectra was obtained. The spectra were obtained with baseline  
200 correction and compared with standard spectra from the database [www.ruff.info](http://www.ruff.info) (atacamite  
201 R050098, brochantite R060133, calcite R040170, cuprite R050384, graphite R050503, gypsum  
202 R040029, murdochite R110122).  
203

### 204 **2.2.3 XRD**

205 The XRD analyses were performed on the same samples examined with Raman spectroscopy. The  
206 samples were analysed by using a diffractometer Rigaku model Mini Flex with Cu-K $\alpha$  radiation ( $\lambda =$   
207  $0.154\text{ nm}$ ). The measurements were carried out with 30 kV accelerating voltage, 15 mA current, scan  
208 angle in  $2\theta$  from  $10^\circ$  to  $80^\circ$ , with step size of  $0.01^\circ$  and scan speed of  $0.05^\circ\cdot\text{s}^{-1}$ . Three scans for each  
209 measurement were performed. XRD patterns were manually compared with standards XRD patterns  
210 from the database [www.ruff.info](http://www.ruff.info) (atacamite R050098, brochantite R060133, calcite R040170,  
211 cuprite R050384, graphite R050503, gypsum R040029, murdochite R110122).  
212

### 3. Result and Discussion

#### 3.1 ED-XRF analysis

Experimental results of ED-XRF analysis carried out on the *patinas* of the *Sant'Oronzo* statue are summarized in [Table 1](#).

Green *patina*, exposed to leaching (sample n. 01), shows copper ( $65\pm 2$  % wt) as main element and sulphur ( $20\pm 2$  % wt) as secondary element. Green *patina* on the mantle (sample n. 09) and the greenish dripping on the right arm (sample n. 06) have different composition.

Dark *patinas*, not exposed to leaching (samples n. 05, 07, 10, 11, 13 and 15), shows copper as main element and chlorine as secondary element. Moreover, the dark *patina* with red dripping on the bottom right mantle (sample n. 12) shows higher sulphur concentration ( $11.5\pm 1.0$  % wt) and iron ( $1.5\pm 0.5$  % wt) as in trace element. Red *patinas*, exposed to leaching (samples n. 02, 03 and 04), show copper and iron as main element and sulphur as secondary element.

It is important to note that iron is widely present on the surface of statue as minor element or in trace. This is due to the corrosion of the rivets nails added during the last restoration accomplished from 1982 to 1987. In fact, the recent rivet (sample n. 19) shows copper ( $39\pm 2$  % wt) as main element and iron ( $10.0\pm 1.0$  % wt) as secondary element, whereas the rivet (sample n. 20) shows iron ( $27\pm 2$  % wt) as main element and copper ( $12.0\pm 1.0$  % wt) as secondary element.

The original nails show copper (45-56 % wt) as main element. Moreover, the nail n. 16 and n. 18 show chlorine ( $21\pm 2$  % wt) as secondary element, while the nail n. 17 shows sulphur ( $12.0\pm 1.0$  % wt) and chlorine ( $5.0\pm 0.5$  % wt) as secondary elements.

Cleaning tests were also carried out on some measuring points both on areas of the statue (sample n. 01 and n. 15) and on nails (sample n. 16, n. 17 and n. 18) and on rivets (sample n. 19). In any case, the increase of copper concentration was highlighted with a simultaneous decrease in sulphur and chlorine concentration.

#### 3.2 Raman and XRD analysis

Raman spectroscopy offers chemical identification of compounds in order to discriminate the corrosion products of copper or bronze manufacture [6,21–25]. In particular, the Raman signals of copper hydroxychlorides and copper hydroxysulphates can be observed in two main regions: the first at lower wavenumbers, between  $100\text{ cm}^{-1}$  and  $1100\text{ cm}^{-1}$ , includes Cu–O deformation, Cu–Cl deformation and  $\text{SO}_4^{2-}$  deformation. The second, at high wavenumbers, between  $3000\text{ cm}^{-1}$  and  $3700$

296 cm<sup>-1</sup>, includes the Cu–O–H stretching vibrations. In particular, the number of bands in this region  
297 usually reflects the number of different O–H groups present in the structure, except in the case of  
298 strong overlap of the bands. For instance, brochantite (Cu<sub>4</sub>SO<sub>4</sub>(OH)<sub>6</sub>) has six hydroxyl groups  
300 bonded to adjacent sulphate group, and therefore Raman spectroscopy shows six peaks. There is  
301 another region, between 1100 cm<sup>-1</sup> and 3700 cm<sup>-1</sup>, which includes the signals that characterize the  
302 amorphous carbon [26–28], often determined on outdoor copper monuments, as well as C–H  
303 vibrations of organic compounds and the water features present in several hydrated mineral phases.  
304  
305  
306  
307

308 In Table 3 it was tried to assign the type of deformation for each Raman signal obtained in analysed  
309 *patinas* of the statue.  
310

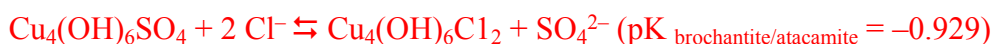
311 Fig. 2a shows the comparison between the Raman spectrum of the green *patina* and of the standard  
312 brochantite. Raman spectrum of green *patina* has the following signals: 120, 140, 200, 242, 318, 390,  
313 420, 450, 485, 506, 595, 609, 622, 910, 975, 1075, 1095, 1125, 1350, 1580, 3265, 3375, 3402, 3489,  
314 3565, 3588 cm<sup>-1</sup>. According to the data reported by scientific literature [29–35] all signals of green  
315 *patina* are attributable to brochantite, except two peaks broader with Raman shift values of about  
316 1350 cm<sup>-1</sup> and 1580 cm<sup>-1</sup>, which are attributable to amorphous carbon and are called D (disorder  
317 band) and G (graphitic band) band, respectively. Moreover, the spectrum of green *patina* shows a  
318 broad band in the range 2800–3000 cm<sup>-1</sup>, which is the region of C–H vibrations of saturated organic  
319 molecules, mainly hydrocarbons and carboxylic acids.  
320  
321  
322  
323  
324  
325

326 Fig. 3a shows the comparison between the Raman spectrum of the dark *patina* and of the standard  
327 atacamite (Cu<sub>2</sub>Cl(OH)<sub>3</sub>). Raman spectrum of dark *patina* has the following signals: 220, 415, 510,  
328 635, 810, 905, 980, 1340, 1600, 2915, 3200, 3355, 3435 cm<sup>-1</sup>. In according to the data reported by  
329 scientific literature, all signals of dark *patina* are attributable to atacamite, in addition to the presence  
330 of amorphous carbon. Moreover, the spectrum shows two broad bands in the range 2800–3000 cm<sup>-1</sup>,  
331 which are the region of C–H vibrations of saturated organic molecules, mainly hydrocarbons and  
332 carboxylic acids.  
333  
334  
335  
336

337 Fig. 4a shows the comparison between the typical Raman spectrum of the sample C04 (green  
338 dripping on Roman capital, West side) and of the standard calcite (CaCO<sub>3</sub>). Raman spectrum of  
339 sample C04 has the following signals: 155, 285, 715, 1085, 1435, 1750, 2625, 2670, 3220 and 3470  
340 cm<sup>-1</sup>. This comparison demonstrated that the sample is mainly composed of calcite and the signals  
341 relating C–H vibrations of saturated organic molecules.  
342  
343  
344

345 XRD analysis prove that both the green *patina* (Fig. 2b) and the dark *patina* (Fig. 3b) contain cuprite  
346 (2θ equal to 29.6, 36.5, 42.3, 61.4, 73.5 and 77.4). This oxide represents the protective layer that  
347 normally covers outdoor copper and bronze monuments. In addition, green *patina* is characterized by  
348 the presence of brochantite, whereas dark *patina* is characterized mainly by the presence of atacamite  
349 more brochantite.  
350  
351  
352  
353  
354

355  
356 Several studies have shown that brochantite is converted into atacamite in solutions containing high  
357 levels of chloride ions through a mechanism of dissolution and precipitation. This chemical-physical  
358 process is reasonable considering the different solubility of the two compounds and their stability  
359 ratio:  
360



364  
365  
366 XRD pattern of the sample C01 (dark dripping on concrete pulvino) shows the presence mainly of  
367 calcite and gypsum, typical compounds used in cementitious material in the form of powders, and of  
368 murdochite ( $\text{Cu}_6\text{PbO}_8$ ). Fig. S5 shows the XRD spectrum of sample C01. The existence of  
369 murdochite on pulvino can be justified considering the corrosion of the lead plate placed at the  
370 pedestal of the statue on which the wooden structure rests.  
371

372  
373  
374 XRD pattern of the sample C02 (green dripping on concrete pulvino) shows the presence mainly of  
375 calcite. The weak signal at  $2\theta$  equal to  $16.2^\circ$  is due to atacamite, confirming that its drip from the  
376 copper statue is the cause of the green coloured areas. The sample C03 (dark dripping on Roman  
377 capital) is also characterized by the presence of calcite as main phase. The dark colour is due both to  
378 the presence of carbon particles and to a dripping of murdochite that comes from the statue's  
379 pedestal. The sample C04 (green dripping on Roman capital) is mainly characterized by calcite (Fig.  
380 4b). The light green colouring on the capital could be due to brochantite of coming from the metallic  
381 statue.  
382

383  
384  
385 The sample C05 (dark area not exposed to washouts on Roman capital) shows the presence of  
386 gypsum as the main phase and calcite. The graphite signal is also present and this may be due to  
387 carbon particles deposited in not washed region, which determine the dark colour.  
388

389  
390  
391 The results obtained by using XRD confirm the results obtained by Raman spectroscopy.  
392

#### 393 394 395 396 **4. Conclusion**

397  
398  
399  
400 Green *patinas* were constituted mainly by cuprite and brochantite, while dark *patinas* were  
401 constituted mainly by cuprite, brochantite and atacamite. The presence of atacamite in areas not  
402 directly exposed to rain may be due probably to deposits of marine spray accumulated in these  
403 sheltered regions of the statue.  
404

405  
406 Furthermore, all the *patinas* contain amorphous carbon which demonstrates the presence of carbon  
407 deposits. In particular, the highest concentration of amorphous carbon was detected in the sheltered  
408 dark *patinas*.  
409

414  
415 The improper use of the rivets used in the last restoration from 1982 to 1987 has irreversibly  
416 damaged the analysed monument, thus modifying its aesthetics (with evident red areas around each  
417 rivet and red dripping starting from the rivet).  
418

419  
420 The simultaneous use of the analytical techniques has allowed to define the compounds of  
421 degradation of *patinas* and the information obtained was of fundamental importance for the  
422 subsequent work of the restorers.  
423  
424

## 425 426 **Acknowledgments**

427  
428  
429 The authors thank Massimo Luggeri (Dipartimento di Scienze e Tecnologie Biologiche e Ambientali,  
430 Università del Salento), who has contributed to improving the quality of the figures. We are grateful  
431 to Company Colaci Emilio Impianti e Restauri (Alessano, Lecce, Italy) and the restorer Elisabetta  
432 Palmiero for promoting this study and for his continuous collaboration. We are also very grateful to  
433 Arch. Maria Piccarreta (*Soprintendenza archeologia belle arti e paesaggio per le province di*  
434 *Brindisi, Lecce e Taranto*) for her always collaborative attitude.  
435  
436  
437  
438  
439

## 440 441 **References**

- 442  
443 [1] G.M. Ingo, T. De Caro, C. Riccucci, E. Angelini, S. Grassini, S. Balbi, P. Bernardini, D. Salvi, L.  
444 Bousselmi, A. Çilingiroğlu, M. Gener, V.K. Gouda, O.A.L. Jarrah, S. Khosroff, Z. Mahdjoub, Z.A.L.  
445 Saad, W. El-Saddik, P. Vassiliou, Large scale investigation of chemical composition, structure and  
446 corrosion mechanism of bronze archeological artefacts from Mediterranean basin, *Appl. Phys. A*  
447 *Mater. Sci. Process.* 83 (2006) 513–520. doi:10.1007/s00339-006-3550-z.  
448 [2] D.E. Couture-Rigert, P.J. Sirois, E.A. Moffatt, An investigation into the cause of corrosion on indoor  
449 bronze sculpture, *Stud. Conserv.* 57 (2012) 142–163. doi:10.1179/2047058412Y.0000000004.  
450 [3] X. Zhang, I. Odnevall Wallinder, C. Leygraf, Mechanistic studies of corrosion product flaking on  
451 copper and copper-based alloys in marine environments, *Corros. Sci.* 85 (2014) 15–25.  
452 doi:10.1016/j.corsci.2014.03.028.  
453 [4] G. Masi, J. Esvan, C. Josse, C. Chiavari, E. Bernardi, C. Martini, M.C. Bignozzi, N. Gartner, T. Kosec,  
454 L. Robbiola, Characterization of typical patinas simulating bronze corrosion in outdoor conditions,  
455 *Mater. Chem. Phys.* 200 (2017) 308–321. doi:10.1016/j.matchemphys.2017.07.091.  
456 [5] R.A. Livingston, Influence of the Environment on the Patina of the Statue of Liberty, *Environ. Sci.*  
457 *Technol.* 25 (1991) 1400–1408. doi:10.1021/es00020a006.  
458 [6] W. Martens, R.L. Frost, J.T. Kloprogge, P.A. Williams, Raman spectroscopic study of the basic copper  
459 sulphates - Implications for copper corrosion and “bronze disease,” *J. Raman Spectrosc.* 34 (2003)  
460 145–151. doi:10.1002/jrs.969.  
461 [7] R.L. Frost, P.A. Williams, J.T. Kloprogge, W. Martens, Raman spectroscopy of the copper chloride  
462 minerals nantokite, eriochalcite and claringbullite – implications for copper corrosion, *Neues Jahrb.*  
463 *Für Mineral. - Monatshefte.* 2003 (2003) 433–445. doi:10.1127/0028-3649/2003/2003-0433.  
464 [8] V. Hayez, V. Costa, J. Guillaume, H. Terryn, A. Hubin, Micro Raman spectroscopy used for the study  
465 of corrosion products on copper alloys: Study of the chemical composition of artificial patinas used for  
466 restoration purposes, *Analyst.* 130 (2005) 550–556. doi:10.1039/b419080g.  
467 [9] X.D. Liu, D.D. Meng, X.G. Zheng, M. Hagihala, Q.X. Guo, Mid-IR and Raman Spectral Properties of  
468 Clinoatacamite-Structure Basic Copper Chlorides, *Adv. Mater. Res.* 146–147 (2010) 1202–1205.  
469 doi:10.4028/www.scientific.net/AMR.146-147.1202.  
470 [10] A.R. Mendoza, F. Corvo, A. Gómez, J. Gómez, Influence of the corrosion products of copper on its  
471 atmospheric corrosion kinetics in tropical climate, *Corros. Sci.* 46 (2004) 1189–1200.  
472

- 473  
474  
475  
476  
477  
478  
479  
480  
481  
482  
483  
484  
485  
486  
487  
488  
489  
490  
491  
492  
493  
494  
495  
496  
497  
498  
499  
500  
501  
502  
503  
504  
505  
506  
507  
508  
509  
510  
511  
512  
513  
514  
515  
516  
517  
518  
519  
520  
521  
522  
523  
524  
525  
526  
527  
528  
529  
530  
531
- doi:10.1016/j.corsci.2003.09.014.
- [11] A.M. Pollard, R.G. Thomas, P.A. Williams, Connellite : stability relationships with other secondary copper minerals, 54 (1990) 425–430.
- [12] G. Di Carlo, C. Giuliani, C. Riccucci, M. Pascucci, E. Messina, G. Fierro, M. Lavorgna, G.M. Ingo, Artificial patina formation onto copper-based alloys: Chloride and sulphate induced corrosion processes, *Appl. Surf. Sci.* 421 (2017) 120–127. doi:10.1016/j.apsusc.2017.01.080.
- [13] J.T. Jambor, John L.; Dutrizac, John E.; Roberts, Andrew C.; Grice, Joel D.; Szymanski, Clinoatacamite, a new polymorph of  $\text{Cu}_2(\text{OH})_3\text{Cl}$ , and its relationship to paratacamite and “anarakite,” *Can. Mineral.* 34 (1996) 61–72.
- [14] R.W. Revie, Uhlig ' S Corrosion Handbook the Electrochemical Society Series, 2011. doi:10.1002/9780470872864.ch39.
- [15] L.S. Selwyn, N.E. Binnie, J. Poitras, M.E. Laver, D.A. Downham, Outdoor Bronze Statues: Analysis of Metal and Surface Samples, *Stud. Conserv.* 41 (1996) 205. doi:10.2307/1506541.
- [16] M. Rita Perrone, A. Turnone, A. Buccolieri, G. Buccolieri, Particulate matter characterization at a coastal site in south-eastern Italy, *J. Environ. Monit.* 8 (2006) 183–190. doi:10.1039/B513306H.
- [17] A. Buccolieri, G. Buccolieri, N. Cardellicchio, A. Dell'Atti, E.T. Florio, PM-10 and heavy metals in particulate matter of the province of Lecce (Apulia, Southern Italy), *Ann. Chim.* 95 (2005). doi:10.1002/adic.200590004.
- [18] A. Buccolieri, A. Castellano, E. Degl'Innocenti, R. Cesareo, R. Casciaro, G. Buccolieri, EDXRF analysis of gold jewelry from the Archaeological Museum of Taranto, Italy, *X-Ray Spectrom.* 46 (2017). doi:10.1002/xrs.2761.
- [19] A. Buccolieri, E. Degl'Innocenti, R. Cesareo, A. Castellano, G. Buccolieri, Non-invasive in-situ analysis of a wreath of gold leaves from the National Archaeological Museum of Taranto, Italy, *Meas. J. Int. Meas. Confed.* 126 (2018) 164–167. doi:10.1016/j.measurement.2018.05.063.
- [20] G. Buccolieri, A. Buccolieri, P. Donati, M. Marabelli, A. Castellano, Nuclear Instruments and Methods in Physics Research B Portable EDXRF investigation of the patinas on the Riace Bronzes, *Nucl. INSTRUMENTS METHODS Phys.* 343 (2015) 101–109. doi:10.1016/j.nimb.2014.11.064.
- [21] R.L. Frost, W. Martens, J. Theo Kloprogge, P.A. Williams, Raman spectroscopy of the basic copper chloride minerals atacamite and paratacamite: Implications for the study of copper, brass and bronze objects of archaeological significance, *J. Raman Spectrosc.* 33 (2002) 801–806. doi:10.1002/jrs.921.
- [22] R.L. Frost, W.N. Martens, L. Rintoul, E. Mahmutagic, J.T. Kloprogge, Raman spectroscopic study of azurite and malachite at 298 and 77 K, *J. Raman Spectrosc.* 33 (2002) 252–259. doi:10.1002/jrs.848.
- [23] R.L. Frost, P.A. Williams, W. Martens, P. Leverett, J.T. Kloprogge, Raman spectroscopy of basic copper(II) and some complex copper(II) sulfate minerals: Implications for hydrogen bonding, *Am. Mineral.* 89 (2004) 1130–1137. doi:10.2138/am-2004-0726.
- [24] G. Bertolotti, D. Bersani, P.P. Lottici, M. Alesiani, T. Malcherek, J. Schlüter, Micro-Raman study of copper hydroxychlorides and other corrosion products of bronze samples mimicking archaeological coins, *Anal. Bioanal. Chem.* 402 (2012) 1451–1457. doi:10.1007/s00216-011-5268-9.
- [25] R.L. Frost, R. Scholz, A. López, Y. Xi, C. Lana, Vibrational spectroscopy of the sulphate mineral sturmanite from Kuruman manganese deposits, South Africa, *Spectrochim. Acta - Part A Mol. Biomol. Spectrosc.* 133 (2014) 24–30. doi:10.1016/j.saa.2014.04.115.
- [26] T. Catelani, G. Pratesi, M. Zoppi, Raman characterization of ambient airborne soot and associated mineral phases, *Aerosol Sci. Technol.* 48 (2014) 13–21. doi:10.1080/02786826.2013.847270.
- [27] C. Brolly, J. Parnell, S. Bowden, Raman spectroscopy: Caution when interpreting organic carbon from oxidising environments, *Planet. Space Sci.* 121 (2016) 53–59. doi:10.1016/j.pss.2015.12.008.
- [28] A. Coccato, J. Jehlicka, L. Moens, P. Vandenabeele, Raman spectroscopy for the investigation of carbon-based black pigments, *J. Raman Spectrosc.* 46 (2015) 1003–1015. doi:10.1002/jrs.4715.
- [29] M. Schmidt, H.D. Lutz, Hydrogen bonding in basic copper salts: a spectroscopic study of malachite,  $\text{Cu}_2(\text{OH})_2\text{CO}_3$ , and brochantite,  $\text{Cu}_4(\text{OH})_6\text{SO}_4$ , *Phys. Chem. Miner.* 20 (1993) 27–32. doi:10.1007/BF00202247.
- [30] M. Bouchard, D.C. Smith, Catalogue of 45 reference Raman spectra of minerals concerning research in art history or archaeology, especially on corroded metals and coloured glass, *Spectrochim. Acta - Part A Mol. Biomol. Spectrosc.* 59 (2003) 2247–2266. doi:10.1016/S1386-1425(03)00069-6.
- [31] R.L. Frost, Raman spectroscopy of selected copper minerals of significance in corrosion, *Spectrochim. Acta - Part A Mol. Biomol. Spectrosc.* 59 (2003) 1195–1204. doi:10.1016/S1386-1425(02)00315-3.
- [32] P. Makreski, G. Jovanovski, S. Dimitrovska, Minerals from Macedonia: XIV. Identification of some sulfate minerals by vibrational (infrared and Raman) spectroscopy, *Vib. Spectrosc.* 39 (2005) 229–239.

532  
533  
534  
535  
536  
537  
538  
539  
540  
541  
542  
543  
544  
545  
546  
547  
548  
549  
550  
551  
552  
553  
554  
555  
556  
557  
558  
559  
560  
561  
562  
563  
564  
565  
566  
567  
568  
569  
570  
571  
572  
573  
574  
575  
576  
577  
578  
579  
580  
581  
582  
583  
584  
585  
586  
587  
588  
589  
590

doi:10.1016/j.vibspec.2005.04.008.

- [33] M.D. Lane, Mid-infrared emission spectroscopy of sulfate and sulfate-bearing minerals, *Am. Mineral.* 92 (2007) 1–18. doi:10.2138/am.2007.2170.
- [34] K. Ben Mabrouk, T.H. Kauffmann, H. Aroui, M.D. Fontana, Raman study of cation effect on sulfate vibration modes in solid state and in aqueous solutions, *J. Raman Spectrosc.* 44 (2013) 1603–1608. doi:10.1002/jrs.4374.
- [35] A. Coccato, D. Bersani, A. Coudray, J. Sanyova, L. Moens, P. Vandenabeele, Raman spectroscopy of green minerals and reaction products with an application in Cultural Heritage research, *J. Raman Spectrosc.* 47 (2016) 1429–1443. doi:10.1002/jrs.4956.

## AUTHOR INFORMATION

### ORCID ID:

Buccolieri Giovanni: <http://orcid.org/0000-0001-8672-9238>

Alfredo Castellano: <http://orcid.org/0000-0002-3107-5836>

Antonio Serra: <http://orcid.org/0000-0003-3380-7751>

Giorgio Zavarise: <http://orcid.org/0000-0002-6340-0015>

Buccolieri Alessandro: <http://orcid.org/0000-0002-8657-9468>

591  
592  
593  
594  
595  
596  
597  
598  
599  
600  
601  
602  
603  
604  
605  
606  
607  
608  
609  
610  
611  
612  
613  
614  
615  
616  
617  
618  
619  
620  
621  
622  
623  
624

### Caption of the Figures

**Fig. 1.** Images of the *Sant'Oronzo* statue (a) and degraded areas of copper *patinas* (b, c and d), of the Roman column (e, f and g) and the concrete base (h). The figure also shows the seven sampling points, which provided the samples analysed both with Raman and XRD.

**Fig. 2.** Typical Raman spectrum (a) and XRD pattern (b) of the green *patina* compared with brochantite standard.

**Fig. 3.** Typical Raman spectrum (a) and XRD pattern (b) of the dark *patina* compared with atacamite standard.

**Fig. 4.** Typical Raman spectrum (a) and XRD pattern (b) of the sample C04 compared with calcite standard.

**Fig. S1.** Image from above (a) and front (b) of the original nails of the *Sant'Oronzo* statue.

**Fig. S2.** Rivet fixing technique.

**Fig. S3.** Image of evidence of rivets on the statue.

**Fig. S4.** Image of the *Sant'Oronzo* statue in the room where it will be restored.

**Fig. S5.** XRD pattern of the sample C01.

625  
626  
627  
628  
629  
630  
631  
632  
633  
634  
635  
636  
637  
638  
639  
640  
641  
642  
643  
644  
645  
646  
647  
648  
649

### Caption of the Tables

**Table 1.** ED-XRF analysis results of different *patinas* on the *Sant'Oronzo* statue.

**Table 2.** Description of the seven samples analysed by Raman spectroscopy and XRD and main compounds detected

**Table 3.** Raman peaks obtained from *patinas* on the *Sant'Oronzo* statue and their possible assignment.

650  
651  
652  
653  
654  
655  
656  
657  
658  
659  
660  
661  
662  
663  
664  
665  
666  
667  
668  
669  
670  
671  
672  
673  
674  
675  
676  
677  
678  
679  
680  
681  
682  
683  
684  
685  
686  
687  
688  
689  
690  
691  
692  
693  
694  
695  
696  
697  
698  
699  
700  
701  
702  
703  
704  
705  
706  
707  
708

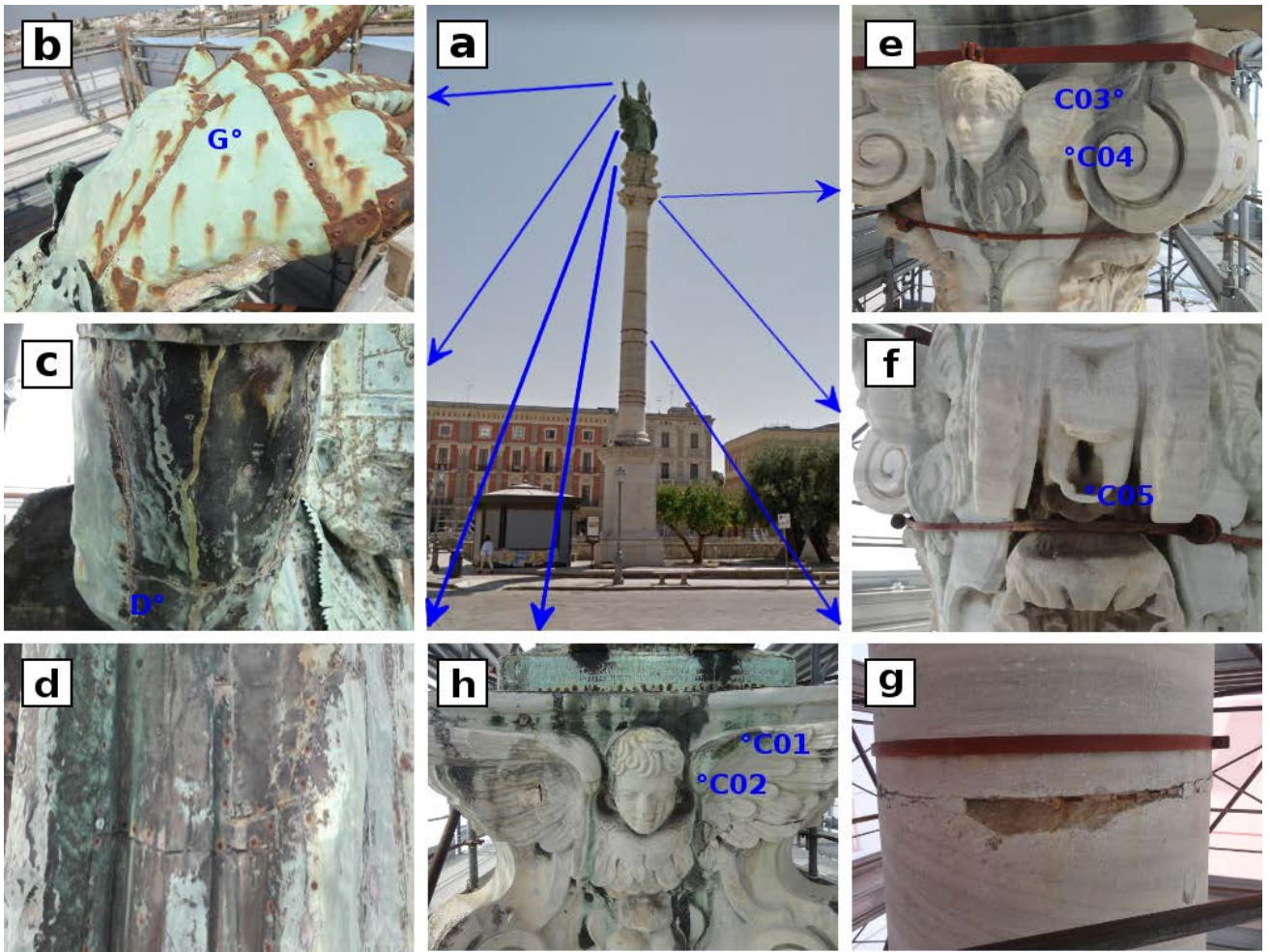


Fig. 1

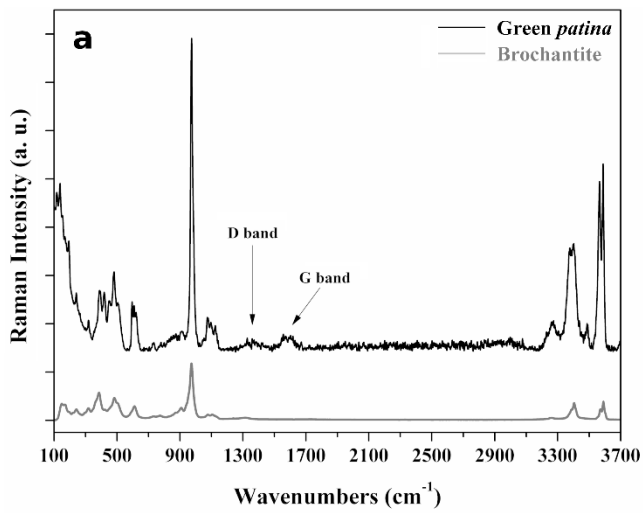


Fig. 2

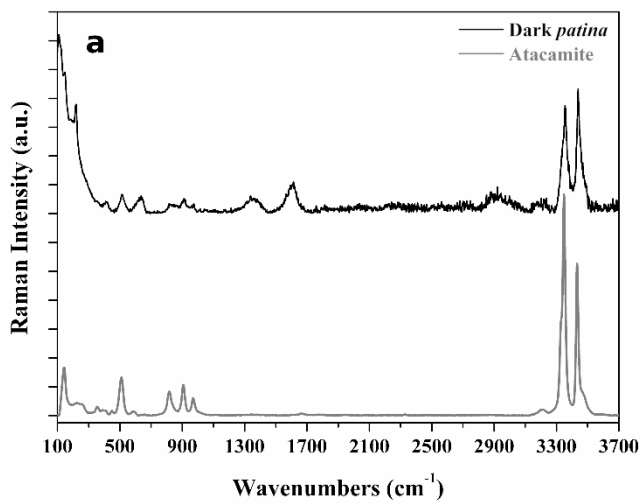


Fig. 3

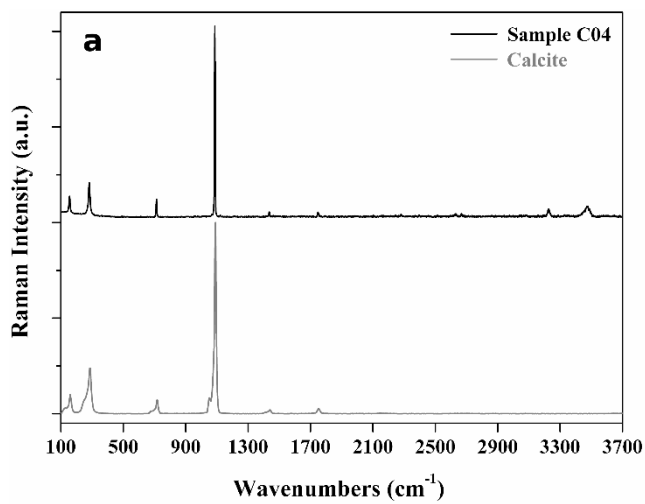


Fig. 4

768  
769  
770  
771  
772  
773  
774  
775  
776  
777  
778  
779  
780  
781  
782  
783  
784  
785  
786  
787  
788  
789  
790  
791  
792  
793  
794  
795  
796  
797  
798  
799  
800  
801  
802  
803  
804  
805  
806  
807  
808  
809  
810  
811  
812  
813  
814  
815  
816  
817  
818  
819  
820  
821  
822  
823  
824  
825  
826

**Table 1**

Sample	Description of sample	Cu	S	Cl	Fe
		(% wt)			
01	Right hand, green <i>patina</i> exposed to leaching	65±2	20±2	<0.5	<0.5
01c	Sample 01 <i>after cleaning</i>	89±2	2.5±0.5	<0.5	1.0±0.5
02	Right hand, red <i>patina</i> exposed to leaching	48.0±1.5	4.4±0.5	<0.5	23±2
03	Right hand, red dripping exposed to leaching	58±2	11.0±1.0	<0.5	4.5±0.5
04	Right hand, red sheet exposed to leaching	87±2	<0.5	<0.5	2.5±0.5
05	Right arm, dark <i>patina</i> sheltered area	50±2	<0.5	23±2	<0.5
06	Right arm, greenish dripping, sheltered area	49±2	17.0±1.5	3.5±0.5	4.0±0.5
07	Dark <i>patina</i> under the mantle, sheltered area	47±2	<0.5	20±2	<0.5
08	Hole on the arm	69±2	7.0±1.0	<0.5	10.0±1.0
09	Mantle, right side, green <i>patina</i> , flat surface	20±2	8.0±1.0	7.0±0.5	<0.5
10	Bottom right mantle, dark <i>patina</i>	45±2	<0.5	19.3±1.5	1.5±0.5
11	Right side, dark <i>patina</i> , sheltered area	48±2	<0.5	16.3±1.5	<0.5
12	Bottom right mantle, dark <i>patina</i> with red dripping	38±2	11.5±1.0	<0.5	1.5±0.5
13	Bottom right base, dark <i>patina</i>	41±2	5.0±0.5	14.0±1.5	<0.5
14	Right side, iron rod	<1.0	<0.5	<0.5	55±2
15	Brown <i>patina</i> , sheltered area	53±2	<0.5	11.0±1.0	<0.5
15c	Sample 15 <i>after cleaning</i>	92±2	<0.5	<0.5	<0.5
16	Right hand, original nail, exposed to leaching	56±2	<0.5	21±2	1.0±0.5
16c	Sample 16 <i>after cleaning</i>	90±2	<0.5	1.5±0.5	1.0±0.5
17	Original nail with green head	52±2	12.0±1.0	5.0±0.5	<0.5
17c	Sample 17 <i>after cleaning</i>	91±2	<0.5	<0.5	<0.5
18	Original nail with dark head	45±2	<0.5	21±2	<0.5
18c	Sample 18 <i>after cleaning</i>	91±2	<0.5	<0.5	<0.5
19	Right hand, recent red rivet, exposed to leaching	39±2	<0.5	1.0±0.5	10.0±1.0
19c	Sample 19 <i>after cleaning</i>	89±2	<0.5	<0.5	8.0±1.0
20	Right hand, red rivet, exposed to leaching	12.0±1.0	<0.5	<0.5	27±2

827  
828  
829  
830  
831  
832  
833  
834  
835  
836  
837  
838  
839  
840  
841  
842  
843  
844  
845  
846  
847  
848  
849  
850  
851  
852  
853  
854  
855  
856  
857  
858  
859  
860  
861  
862  
863  
864  
865  
866  
867  
868  
869  
870  
871  
872  
873  
874  
875  
876  
877  
878  
879  
880  
881  
882  
883  
884  
885

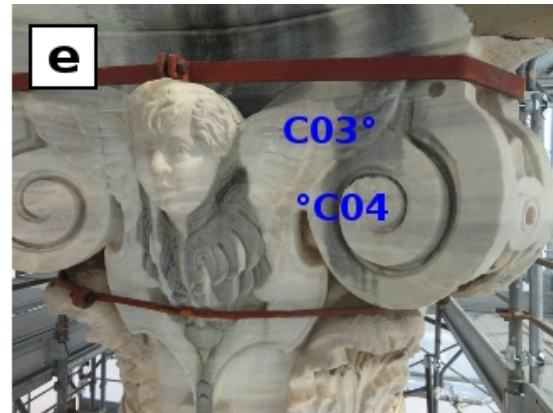
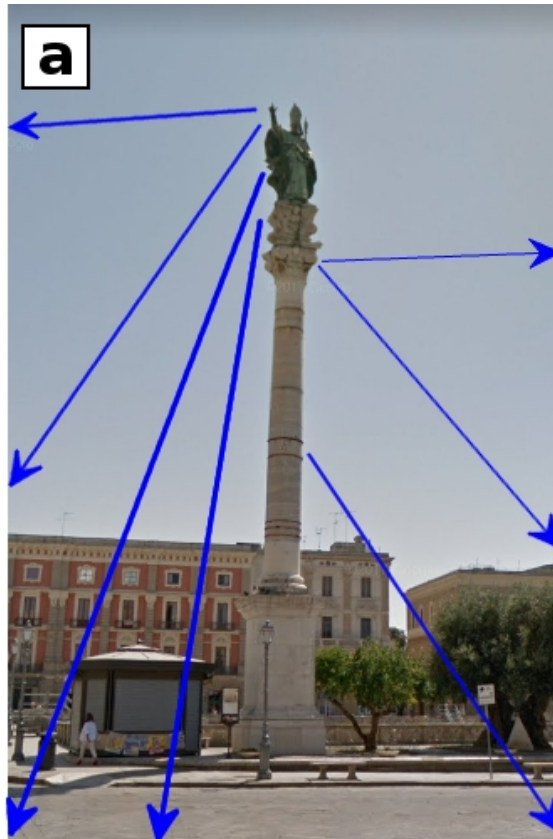
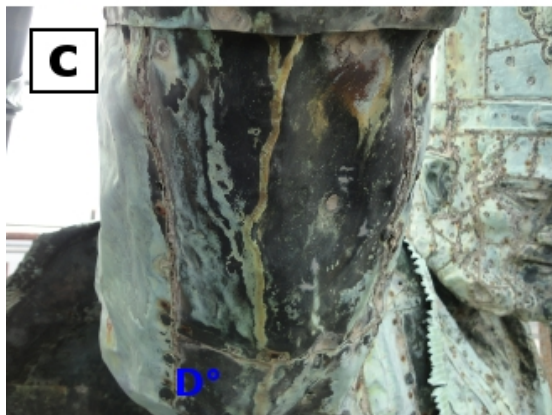
**Table 2**

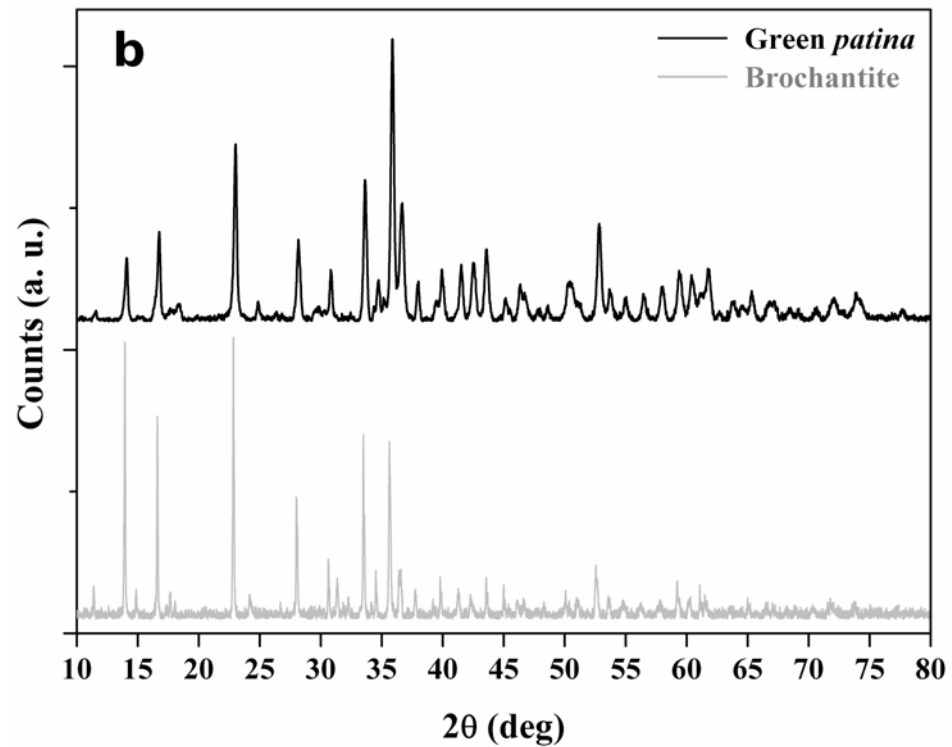
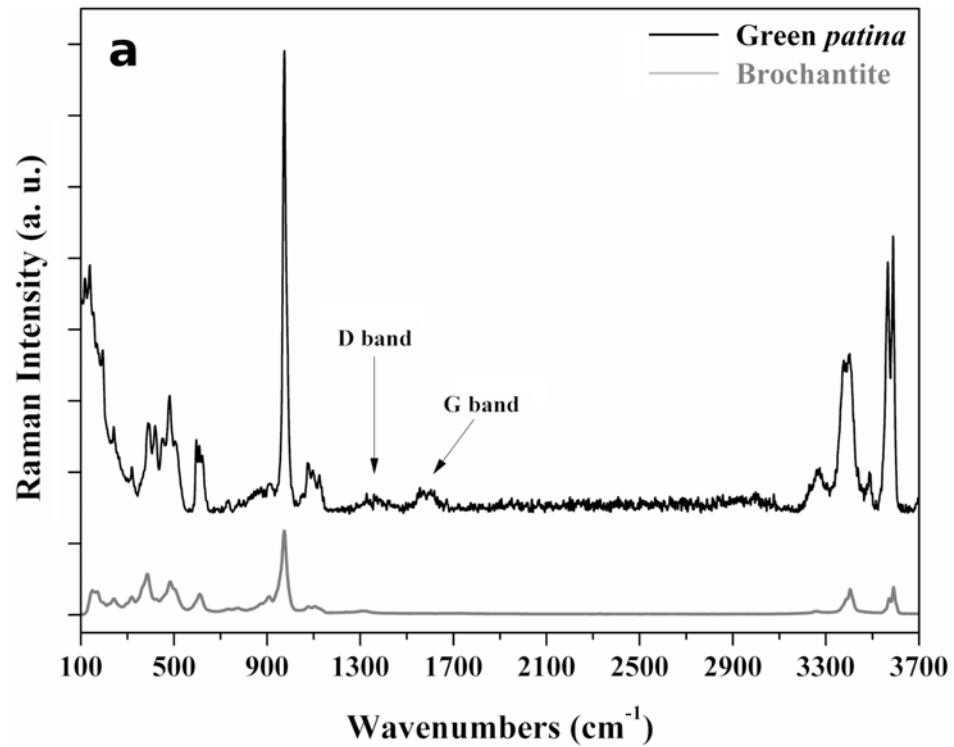
Sample	Description of sample	Main compounds determined	
		by Raman	by XRD
<b>G</b>	Right hand, green sheet, exposed to leaching	Brochantite	Brochantite, Cuprite
<b>D</b>	Right arm, dark sheet, sheltered area	Atacamite	Atacamite, Cuprite
<b>C01</b>	Dark dripping on concrete pulvino, South side	Calcite	Calcite, Gypsum, Murdochite
<b>C02</b>	Green dripping on concrete pulvino, South side	Calcite	Calcite, Atacamite
<b>C03</b>	Dark dripping on Roman capital, West side	Calcite	Calcite, Murdochite
<b>C04</b>	Green dripping on Roman capital, West side	Calcite	Calcite
<b>C05</b>	Dark area on Roman capital (volute), North-West side	Gypsum	Gypsum

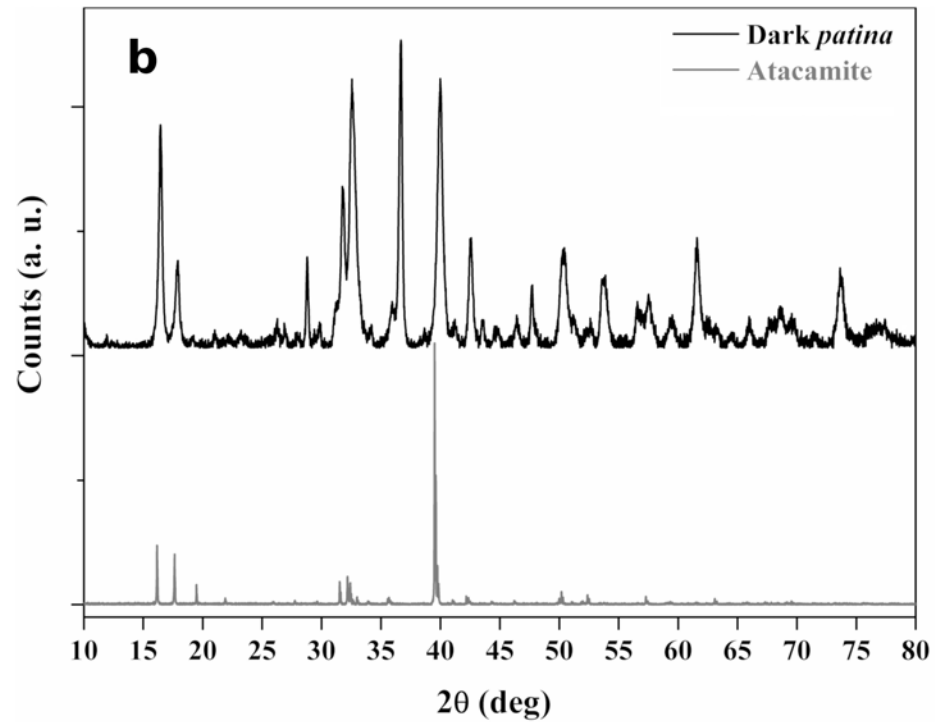
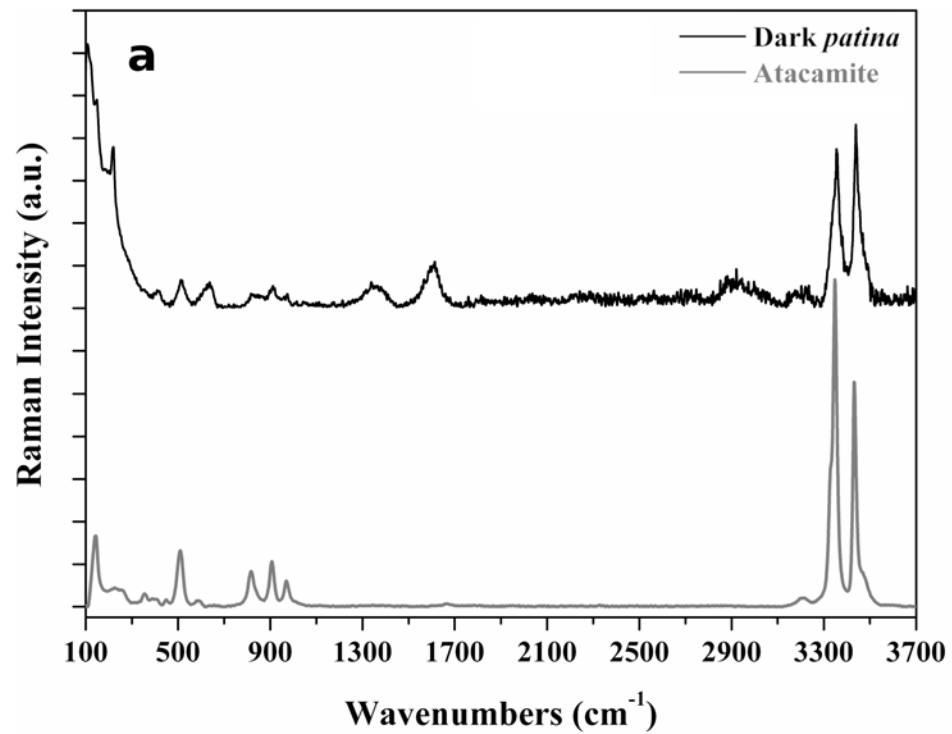
**Table 3**

886  
887  
888  
889  
890  
891  
892  
893  
894  
895  
896  
897  
898  
899  
900  
901  
902  
903  
904  
905  
906  
907  
908  
909  
910  
911  
912  
913  
914  
915  
916  
917  
918  
919  
920  
921  
922  
923  
924  
925  
926  
927  
928  
929  
930  
931  
932  
933  
934  
935  
936  
937  
938  
939  
940  
941  
942  
943  
944

Wavenumber (cm <sup>-1</sup> )	Suggested assignment
120 140	Cu–O bending
155	(Ca <sup>2+</sup> , CO <sub>3</sub> <sup>2-</sup> ) lattice modes
200	Cu–Cl bending
225	Cu–O bending
242	Cu–Cl bending
285	(Ca <sup>2+</sup> , CO <sub>3</sub> <sup>2-</sup> ) lattice modes
318 390 420	Cu–Cl stretching
450	SO <sub>4</sub> <sup>2-</sup> symmetric bending
485 506	Cu–O symmetric stretching
520	Cu–OH symmetric stretching
595 609 622	SO <sub>4</sub> <sup>2-</sup> anti-symmetric bending
625	Cu–O symmetric stretching
715	CO <sub>3</sub> <sup>2-</sup> symmetric stretching
808 825 910 975	OH deformation
975	SO <sub>4</sub> <sup>2-</sup> symmetric stretching
1075 1095 1125	SO <sub>4</sub> <sup>2-</sup> anti-symmetric stretching
1085	CO <sub>3</sub> <sup>2-</sup> symmetric stretching
1350	disorder carbon ( <i>band D</i> )
1580	graphitic carbon ( <i>band G</i> )
1435	CO <sub>3</sub> <sup>2-</sup> asymmetric stretching
1750	CO <sub>3</sub> <sup>2-</sup> symmetric stretching
3260 3375 3405 3490 3565 3585	Cu–OH hydroxyl stretching



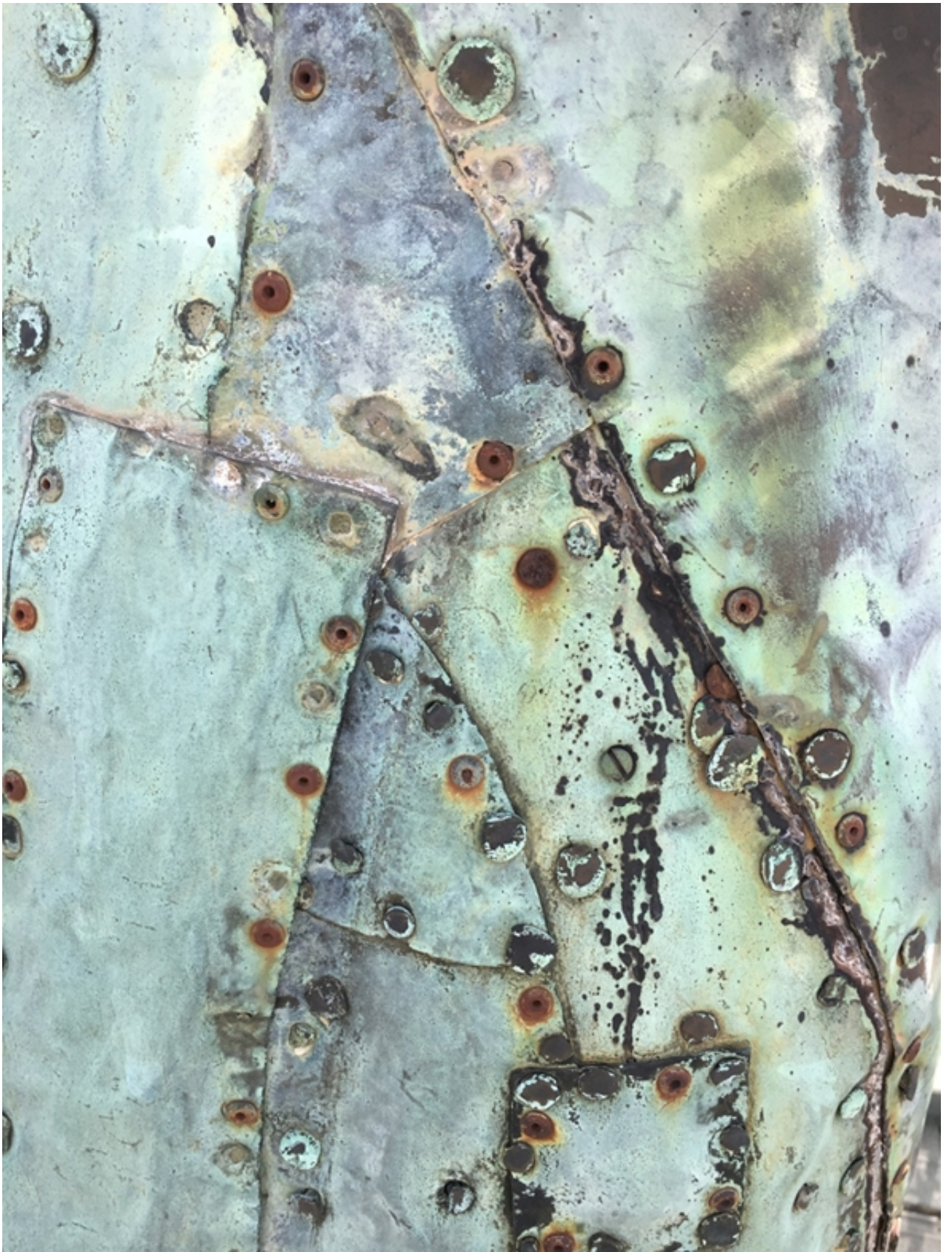




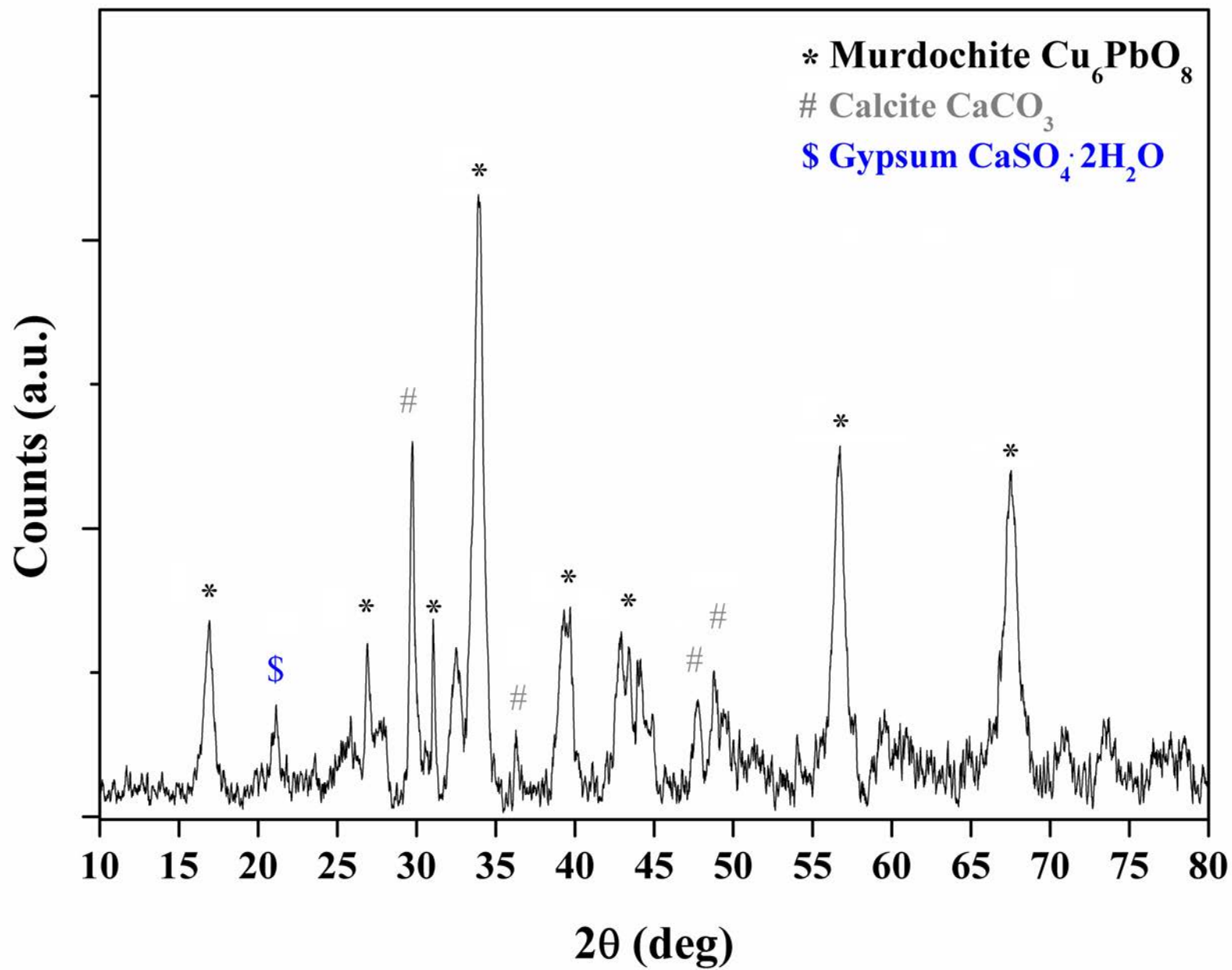












## CONFLICT OF INTEREST

Manuscript title: **Archaeometric analysis of *patinas* of the outdoor copper statue *Sant'Oronzo* (Lecce, Italy) preparatory to the restoration**

Corresponding author's full name:	<b>Alessandro Buccolieri</b>
-----------------------------------	------------------------------

List of the authors:

<b>N.</b>	<b>Author's full name</b>
1.	Giovanni Buccolieri
2.	Alfredo Castellano
3.	Antonio Serra
4.	Giorgio Zavarise
5.	Elisabetta Palmiero
6.	Alessandro Buccolieri

*All authors declare that they have no conflict of interest for the publication of the manuscript.*

Lecce, 14<sup>th</sup> November 2019

Corresponding author's signature  
(Alessandro Buccolieri)



## AUTHORS STATEMENT FOR PUBLICATION

Manuscript title: **Archaeometric analysis of *patinas* of the outdoor copper statue *Sant'Oronzo* (Lecce, Italy) preparatory to the restoration**

Corresponding author's full name:	<b>Alessandro Buccolieri</b>
-----------------------------------	------------------------------

*List of the authors:*

No.	Author's full name
1.	Giovanni Buccolieri
2.	Alfredo Castellano
3.	Antonio Serra
4.	Giorgio Zavarise
5.	Elisabetta Palmiero
6.	Alessandro Buccolieri

Component of the research	Author's number
substantial contribution to conception and design	1 2 3 4 5 6
substantial contribution to acquisition of data	1 2 3 4 5 6
substantial contribution to analysis and interpretation of data	1 2 3 4 5 6
drafting the article	1 2 3 4 5 6
critically revising the article for important intellectual content	1 2 3 4 5 6
final approval of the version to be published	1 2 3 4 5 6

Please tick the box if the statement applies:

to the best of your knowledge everybody who participated substantially in the study is not omitted from the article

to the best of your knowledge, all persons listed as authors qualify for authorship

All persons who have made substantial contributions to the work but do not meet the criteria for authorship are listed in Acknowledgments section (technical help, writing assistance, general support, financial and material support)

Yes       No

All persons named in the Acknowledgment section of the manuscript have given their permission to be named

Yes       No

**ORIGINALITY OF THE WORK STATEMENT:**

- the manuscript is not previously published in the same or very similar form in other journal (previous publishing does not apply to abstract or poster presentations at a professional meeting)
- the manuscript is not currently under consideration in other journals (that does not apply for manuscripts that have been rejected by other journals)

Therefore, the manuscript has not been published previously, it is not under consideration for publication elsewhere, its publication is approved by all Authors and tacitly or explicitly by the responsible authorities where the work was carried out and, if accepted, it will not be published elsewhere in the same form in English or in any other language without the written consent of the Publisher.

Lecce, 14<sup>th</sup> November 2019

Corresponding author's signature  
(Alessandro Buccolieri)



## Supplementary material

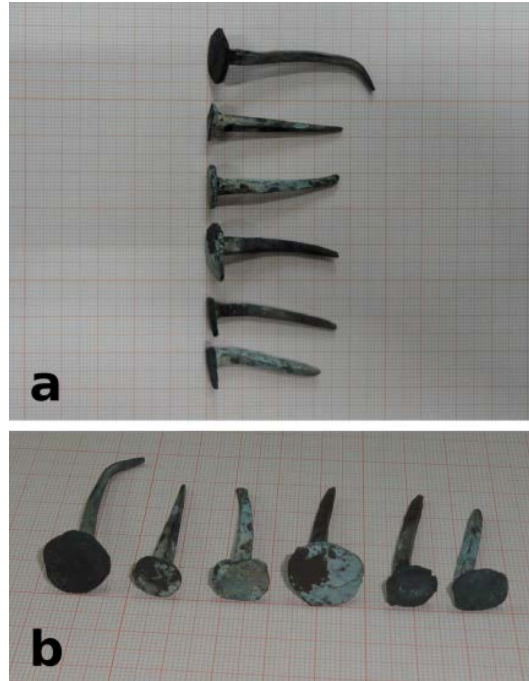


Fig. S1

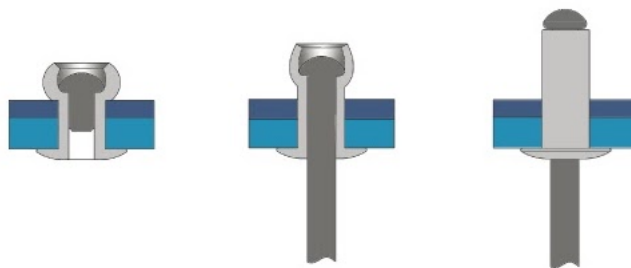


Fig. S2



**Fig. S3**



**Fig. S4**

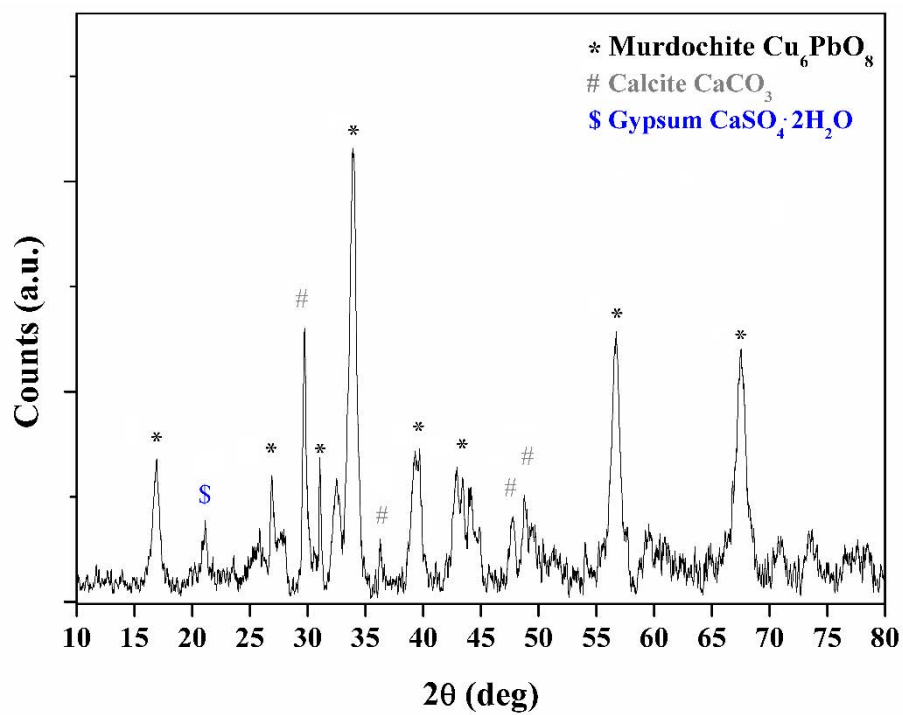


Fig. S5